He*(2^3S) Penning ionization of H_2S. I. Theoretical Franck–Condon factors for the $H_2S(\tilde{X}^1A_1, v'=0) \rightarrow H_2S^+(\tilde{X}^2B_1, \tilde{A}^2A_1)$ ionization and $H_2S^+(\tilde{A}-\tilde{X})$ transition

Ikuo Tokue[a] and Katsuyoshi Yamasaki
Department of Chemistry, Faculty of Science, Niigata University, Ikarashi, Niigata 950-2181, Japan

Shinkoh Nanbu
Research Center for Computational Science, Okazaki National Research Institutes, Myodaiji, Okazaki 444-8585, Japan

(Received 13 May 2003; accepted 26 June 2003)

In order to elucidate the ionization dynamics, in particular the vibrational distribution, of $H_2S^+(\tilde{A})$ produced by the Penning ionization of H_2S with He*(2^3S) atoms, the Franck–Condon factors (FCFs) were presented for the $H_2S(\tilde{X}) \rightarrow H_2S^+(\tilde{X},\tilde{A})$ ionization and the $H_2S^+(\tilde{A}-\tilde{X})$ transition, and Einstein's A coefficients were presented for the latter transition. The FCFs were obtained by quantum vibrational calculations using the global potential energy surfaces (PESs) of $H_2S(\tilde{X}^1A_1)$ and $H_2S^+(\tilde{X}^2B_1, \tilde{A}^2A_1, \tilde{B}^2B_2)$ electronic states. The global PESs were determined by the multireference configuration interaction calculations with the Davidson correction and the interpolant moving least squares method combined with the Shepard interpolation. The obtained FCFs exhibit that the $H_2S^+(\tilde{X})$ state primarily populates the vibrational ground state since its equilibrium geometry is almost equal to that of $H_2S(\tilde{X})$, while the bending mode (ν_2) is strongly enhanced for the $H_2S^+(\tilde{A})$ state; the maximum in the population is around $\nu_2=6-7$. In the same manner, the bending progressions are expected to consist of the great part of the $H_2S^+(\tilde{A}-\tilde{X})$ emission. A detailed comparison with the experimental study for this system is reported in the accompanying paper, Paper II. © *2003 American Institute of Physics.* [DOI: 10.1063/1.1602063]

I. INTRODUCTION

In the Penning ionization of He*(2^3S) with hydrogen sulfide, the $\tilde{X}^2B_1$, $\tilde{A}^2A_1$, and $\tilde{B}^2B_1$ states of the H_2S^+ ion were observed by electron spectroscopy.[1–3] In contrast, no emission from the parent ion was identified by Penning ionization optical spectroscopy.[4,5] Most recently we have assigned the $H_2S^+(\tilde{A}^2A_1-\tilde{X}^2B_1)$ emission produced by the collision of H_2S with the He*(2^3S) atom and have analyzed the vibrational and rotational populations of the $\tilde{A}^2A_1$ state; the details are reported in Paper II. The analysis to elucidate the vibrational populations of the $\tilde{A}$ state requires several types of spectroscopic data such as vibrational and rotational energies, transition probabilities, Franck–Condon factors (FCFs), and Hönl–London factors. Several groups have carried out theoretical calculations for H_2S^+ and iso-electronic species.[6–8] Unfortunately, the published data regarding vibrational energies and FCFs have been found to be inadequate from both experimental and theoretical standpoints for analyzing the observed spectra in our preliminary analysis. Bruna *et al.*[8] have calculated FCFs for the symmetric and antisymmetric stretching and bending modes in the $H_2S^+(\tilde{A}-\tilde{X})$ transition by a one-dimension model. Nevertheless, the vibrational states of the $\tilde{X}$ and $\tilde{A}$ states were found to show large anharmonic characters. We therefore obtained these data by a three-dimensional calculation in the present study.

The topography of the potential energy surface (PES) is the key to understanding Penning ionization processes since a chemical reaction is described by nuclear motion on a PES. Three-dimensional PESs of both the target $H_2S(\tilde{X})$ molecule and the product $H_2S^+(\tilde{X},\tilde{A})$ ions were obtained by an *ab initio* molecular orbital (MO) configuration interaction (CI) method, and three-dimensional transition moments were obtained for the $H_2S^+(\tilde{A}-\tilde{X})$ system. Furthermore, we carried out quantum vibrational calculations on these potential surfaces to obtain the vibrational eigenvalues and eigenfunctions and obtained the FCFs for the $H_2S(\tilde{X}) \rightarrow H_2S^+(\tilde{X},\tilde{A})$ ionization and the $H_2S^+(\tilde{A}-\tilde{X})$ transition.

The present paper outlines first the *ab initio* MO CI calculations used in our determination of the PESs, as well as quantum vibrational calculations. Subsequently, we describe the potential energy surfaces for the $\tilde{X}^2B_1$, $\tilde{A}^2A_1$, and $\tilde{B}^2B_1$ states of H_2S^+ and the ground state of H_2S, and also vibrational states for each electronic state. Finally, the obtained FCFs and Einstein's A coefficients are summarized and discussed in comparison with the other results. The mechanism of the Penning ionization for the He*(2^3S) + H_2S reaction are discussed in Paper II.

[a]Author to whom correspondence should be addressed. Electronic mail: itok-pc@chem.sc.niigata-u.ac.jp

II. THEORETICAL CALCULATIONS

A. *Ab initio* MO CI calculations

Determination of the global PES is quite important to calculations of the higher vibrational states, as it is necessary to take into account the anharmonicity of the PES, especially for the electronic excited states. In other words, most electronic excited states do not possess a single minimum such as the electronic ground state. Therefore, we performed *ab initio* calculations for approximately 4000 molecular conformations on each three-dimensional PES, even for the electronic excited states.

The basis set used in the present work was the diffuse function augmented, correlation consistent, polarized valence, triple zeta (aug-cc-pVTZ) of Woon and Dunning.[9] The MOs were determined by complete active space self-consistent (CASSCF) calculations. After determining the MOs, multireference configuration interaction (MRCI) calculations were carried out.

H_2S is an 18-electron system, and the electronic configuration of the ground state for the valence is

$$(4a_1)^2(2b_2)^2(5a_1)^2(2b_1)^2.$$

The symmetric species of $H_2S(\tilde{X}\,^1A_1)$ is $^1A'$. The three lowest H_2S^+ ion states come out of the three highest occupied orbitals, as follows:

$$\tilde{X}\,^2B_1:(2b_2)^2(5a_1)^2(2b_1)^1,$$

$$\tilde{A}\,^2A_1:(2b_2)^2(5a_1)^1(2b_1)^2,$$

$$\tilde{B}\,^2B_2:(2b_2)^1(5a_1)^2(2b_1)^2.$$

The two lowest $\tilde{X}$ and $\tilde{A}$ states are derived from $^2\Pi_u$ from the Renner–Teller interaction, and the three states correlate with the $H_2(X\,^1\Sigma^+)+S^+(^2D_u)$ system in the dissociation limit. To obtain the MOs necessary to describe these electronic states, the state-averaged CASSCF calculations were carried out with inclusion of a full valence as the active space orbitals. The active space of the MRCI calculations is the same as that of CASSCF, and the configuration state functions were generated by single and double excitations with respect to the reference configurations used in the CASSCF calculation, except for the frozen-core orbitals, $1s$, $2s$, and $2p$ (S). Moreover, the Davidson correction for the MRCI calculation was employed to include the correlation energy due to higher excitations.[10–12] The total number of configurations for the final internally contracted MRCI calculations is approximately 150 000 for the A' symmetry.[13,14] In the present work, the potential energies for the electronic ground state, $1\,^1A'$, of H_2S, and the electronic ground state, $1\,^2A'$, and the next two electronic excited states, $2\,^2A'$ and $1\,^2A''$, of H_2S^+ were finally obtained in the C_s symmetry. All calculations were carried out with the MOLPRO program package.[15] The computer was an SGI Origin 2800 owned by the Research Center for Computational Science at Okazaki.

Potential energies for H_2S and H_2S^+ were calculated at 3600 and 4700 geometries, respectively, and were interpolated by the interpolant moving least squares method combined with the Shepard method[16–18] to carry out a quantum vibrational calculation on the PESs. The parameters to determine the weight functions [see Eq. (6) of Ref. 16] were chosen to be $a=0.03$ and $p=3$.

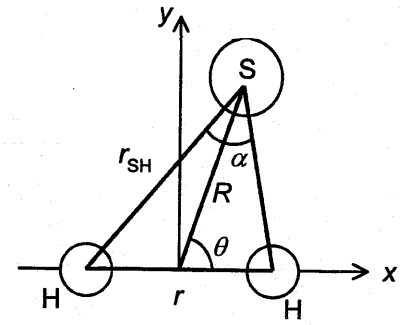

FIG. 1. Jacobi coordinates, bond length-bond angle coordinates, and Cartesian $(x-y)$ coordinates.

B. Quantum vibrational calculations

Since some of the highly vibrational excited states could be characterized with the unlocalized wave function that does not look like the zero-point vibrational wave function, we performed a quantum vibrational calculation based on the discrete variable representations.[19–22] The body-fixed Jacobi coordinates, which are shown in Fig. 1, were employed to describe the relative positions of the three nuclei in the body fixed plane; R is the distance between the S atom and the center of mass of two H atoms, r is the distance between the two H atoms, and the θ is the angle between the vectors R and r.[23] The Hamiltonian matrix and associated wave functions are represented with evenly spaced grids in R and r, and associated Legendre polynominals to describe cos θ. The grid parameters were suitable for the radial part: ($N_R=95$,$R_{\min}$

TABLE I. Equilibrium geometries of H_2S and H_2S^+.

State	Parameter[a]	This work	MRD-CI[b]	Experiment
$H_2S(\tilde{X}\,^1A_1)$	r_{SH}	1.342	···	1.328[c]
	α	92.4	···	92.2[c]
$H_2S^+(\tilde{X}\,^2B_1)$	r_{SH}	1.362	1.364	1.358[d,e]
	α	93.0	92.7	92.5,[d] 92.9[e]
	ΔE_e/eV	10.34	10.17	10.48,[f] 10.43,[g] 10.47,[h] 10.466[i]
$H_2S^+(\tilde{A}\,^2A_1)$	r_{SH}	1.362	1.366	1.376,[d] 1.369[e]
	α	126.8	128.3	128,[d] 127[e]
	ΔE_e/eV	12.63	13.16	12.76,[f] 12.81,[g] 12.78,[h] 12.777[i]
$H_2S^+(\tilde{B}\,^2B_2)$	r_{SH}	1.550	1.593	···
	α	33.8	32.2	···
	ΔE_e/eV	13.42	15.46	14.56,[f] 14.79,[g] 14.78,[h] 14.643[i]

[a]Bond length and angle are in Å and degree units, respectively, and ΔE_e is the energy difference from the $H_2S(\tilde{X}\,^1A_1)$ state.
[b]Reference 8.
[c]Reference 27.
[d]Reference 26.
[e]Reference 28.
[f]Adiabatic ionization potential, Ref. 29.
[g]Reference 30.
[h]Reference 31.
[i]Reference 32.

$=0.0a_0, R_{max}=7.0a_0$) and ($N_r=95, r_{min}=0.0a_0, r_{max}=7.0a_0$), where N is the number of grid points and a_0 is the Bohr radius. The number of Legendre functions was 50 for the angular part. The method adopted for the diagonalization of the Hamiltonian matrix is the implicitly restricted Lanczos method.[24] In the present work, assuming the total angular momentum $J=0$, the lowest 100 vibrational states were obtained for the $A'(^1A_1)$ state of H_2S. Those for the $A'(^2A_1)$ and $A''(^2B_1)$ states of H_2S^+ were calculated up to the 200 states, and the FCFs were then evaluated as the square of the overlap integrals between the initial and final states. The electronic transition probabilities for spontaneous emission[25] were also evaluated for the $H_2S^+(\tilde{A}-\tilde{X})$ transition as the square of the transition moments that depend on both the initial and final vibrational states.

III. RESULTS AND DISCUSSION

A. Potential energy surfaces

The equilibrium geometry of each state was calculated via polynomial fit for the potential energy data. Table I summarizes the geometries thus determined compared with the published data. Our theoretical results agree well with the experimental data. Figure 2 shows the potential surfaces of $H_2S(\tilde{X})$ and $H_2S^+(\tilde{X},\tilde{A})$, where r is fixed at the equilibrium for each state. The energy zero of each electronic state is taken to be at the global energy minimum of the corresponding state; $\tilde{X}\,^1A_1$ of H_2S, and $\tilde{X}\,^2B_1$, $\tilde{A}\,^2A_1$, and $\tilde{B}\,^2B_2$ of H_2S^+ are $-398.940\,676\,77$, $-398.560\,858\,83$, $-398.476\,653\,07$, and $-398.447\,472\,83E_h$, respectively. As shown in Fig. 2, both of the $H_2S(\tilde{X})$ and $H_2S^+(\tilde{X})$ states have the similar topographical feature, indicating that the 0–0 transition should be a dominant process between these states.

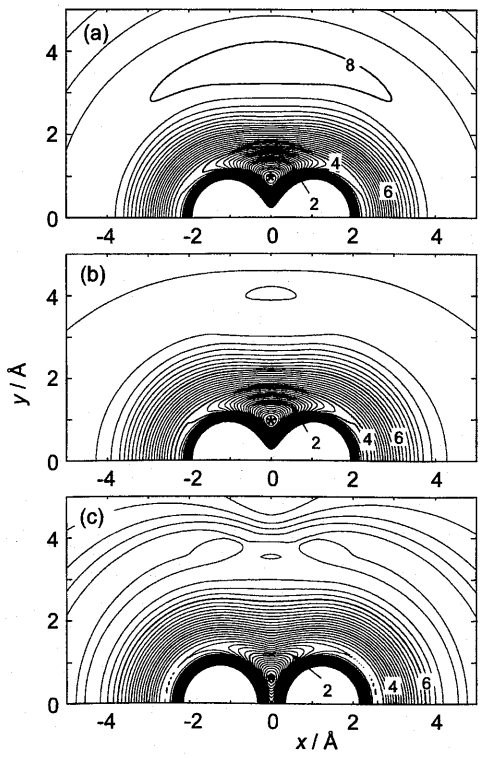

FIG. 2. Potential energy surfaces for (a) $H_2S(\tilde{X})$, (b) $H_2S^+(\tilde{X})$, and (c) $H_2S^+(\tilde{A})$; the r is fixed at the equilibrium distance for each state. The asterisk (*) represents the potential minimum. The numerical values represent the energy differences from each potential minimum in eV. Narrow and thick contours are shown in the interval of 0.2 and 2.0 eV, respectively.

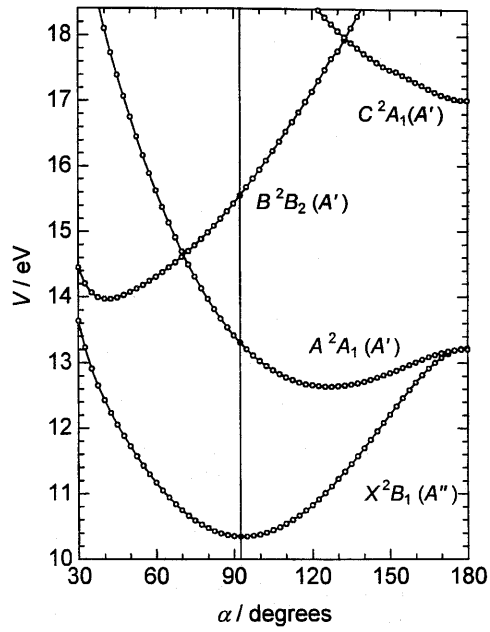

FIG. 3. Potential curves of $H_2S^+(\tilde{X},\tilde{A},\tilde{B})$ for α; r_{SH} is fixed at the equilibrium length of 1.342 Å for $H_2S(\tilde{X})$. The circles show the calculated values. The potential energy, V, means the difference from the minimum for the $H_2S(\tilde{X})$ state. The vertical line near 92° represents the equilibrium angle for $H_2S(\tilde{X})$.

Figure 3 shows the potential energy curves for the three lowest states in H_2S^+, where r_{SH} is fixed at 1.342 Å, which is the equilibrium length for $H_2S(\tilde{X})$. It is clearly seen that there is a Renner–Teller pair of the $\tilde{A}\,^2A_1$ and $\tilde{X}\,^2B_1$ states at around the linear conformation. Although the $\tilde{A}\,^2A_1$ and $\tilde{B}\,^2B_2$ states cross each other at around $\alpha=70°$, these states avoid crossing due to the same symmetry A' because the molecular symmetry comes to the lowest symmetry (C_s). Thus, the vibrational states of the $\tilde{A}\,^2A_1$ and $\tilde{B}\,^2B_2$ states can be mixed due to the nonadiabatic transitions. Furthermore,

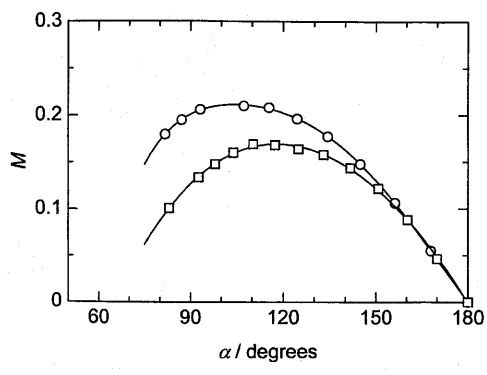

FIG. 4. Electronic transition moments for the $H_2S^+(\tilde{A}-\tilde{X})$ system vs α at $\theta=90°$ and $r=1.9$ Å (circle) and $r=2.4$ Å (square).

TABLE II. Vibrational energies, G, calculated for $H_2S(\tilde{X}\,^1A_1)$ and $H_2S^+(\tilde{X}\,^2B_1,\tilde{A}\,^2A_1)$ and their assignments.[a]

$H_2S(\tilde{X}\,^1A_1)$		$H_2S^+(\tilde{X}\,^2B_1)$		$H_2S^+(\tilde{A}\,^2A_1)$	
(G/cm^{-1})	(ν_1,ν_2,ν_3)	(G/cm^{-1})	(ν_1,ν_2,ν_3)	(G/cm^{-1})	(ν_1,ν_2,ν_3)
0.0	(0,0,0)	0.0	(0,0,0)	0.0	(0,0,0)
1157.6	(0,1,0)	1129.3	(0,1,0)	1028.5	(0,1,0)
2340.7	(0,2,0)	2259.1	(0,2,0)	1945.5	(0,2,0)
2574.0	(1,0,0)	2502.9	(1,0,0)	2463.0	(1,0,0)
2682.7	(0,0,1)	2549.1	(0,0,1)	2482.8	(0,0,1)
3513.1	(0,3,0)	3420.5	(0,3,0)	2720.3	(0,3,0)
3731.2	(1,1,0)	3611.3	(0,1,1)	3355.7	(0,4,0)
3815.4	(0,1,1)	3639.3	(1,1,0)	3476.5	(0,1,1)
4690.8	(0,4,0)	4591.8	(0,4,0)	3491.0	(1,1,0)
4939.3	(1,2,0)	4744.9	(0,2,1)	4036.6	(0,5,0)
4971.2	(0,2,1)	4762.1	(1,2,0)	4361.7	(0,2,1)

[a]The symmetric stretching (ν_1), bending (ν_2), and antisymmetric stretching (ν_3) modes.

the rovibrational mixing of the $\tilde{A}\,^2A_1$ and $\tilde{X}\,^2B_1$ states can occur due to the Renner–Teller coupling, which is also a nonadiabatic process. However, in the present work, keeping the adiabaticity of the electronic states, we applied the Franck–Condon analysis to this system for understanding the Penning ionization mechanism. The $\tilde{B}\,^2B_2$ state was found to cross near 130° with the $\tilde{C}\,^2A_1$ state, which has the S–H antibonding character of σ_s type. Nevertheless, we do not describe the latter state in detail since the purpose of this study is to describe the potential energy surfaces for the lowest three states of H_2S^+.

Figure 4 shows the dependence of the electronic transition moment, M, for the $H_2S^+(\tilde{A}-\tilde{X})$ system on α at $\theta=90°$ and $r=1.9$ and 2.4 Å, which are where the equilibrium geometries are for the $\tilde{X}$ and $\tilde{A}$ states, respectively. The M shows a peak at $\alpha=90°-130°$, which is around the equilibrium angles for both states. Although the M increases with decreasing r and deviating θ from 90°, the contribution from these areas to the pure bending transitions is expected to be small.

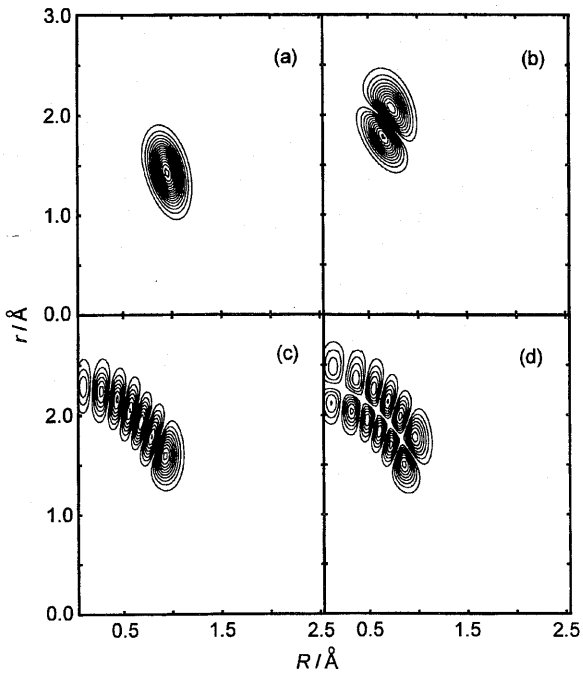

FIG. 5. Vibrational wave functions on the $R-r$ plane at $\theta=90°$ for (a) the first state (0,0,0) of $H_2S(\tilde{X})$, (b) the fourth state (1,0,0), (c) the 15th state (0,6,0), and (d) the 27th state (1,5,0) of $H_2S^+(\tilde{A})$.

B. Vibrational analysis

Table II summarizes the vibrational energies, G, of the lowest 11 states obtained for the $H_2S(\tilde{X})$ and $H_2S^+(\tilde{X}\,^2B_1,\tilde{A}\,^2A_1)$ states with their assignments. Figures 5 and 6 show the vibrational wave functions for these states on the $R-r$ plane at $\theta=90°$. The nodal structures are clearly seen in these figures. The $(0,0,\nu_3'=\text{odd})$ state, which has a node on the plane with $\theta=90°$, is not displayed.

Vibrational frequencies calculated for the $H_2S(\tilde{X})$ and $H_2S^+(\tilde{X},\tilde{A})$ states are compared with experimental data as well as other calculations in Table III. The bending progressions are found to be prominent in the preliminary analysis of the $H_2S^+(\tilde{A}-\tilde{X})$ emission spectra produced by the Penning ionization of H_2S as described in Paper II. To examine the accuracy of the potential surfaces, especially concerning the bending mode, the vibrational frequencies for the $H_2S^+(\tilde{A})$ state obtained in this study are compared with the observed data[26] in Table IV; the deviation from the observed data is evaluated to be within 11%. Because the deviation from the observed energies does not seem to be accumulated in the range higher than 5000 cm^{-1}, the accuracy of the vibrational energies for the $\tilde{X}$ and $\tilde{A}$ states of the ion is roughly estimated to be within 10% up to the (0,10,0) state in this calculation.

For the $H_2S(\tilde{X})$ and $H_2S^+(\tilde{X})$ states, the vibrational quantum numbers have been assigned up to 56 and 77 levels, respectively. To elucidate the anharmonicity of the PES, a least-square analysis was applied to the vibrational frequencies of these levels using the well-known formula for three normal vibrations including anharmonicity constants; the vibrational frequency in reference to the vibrational ground state is given by[27]

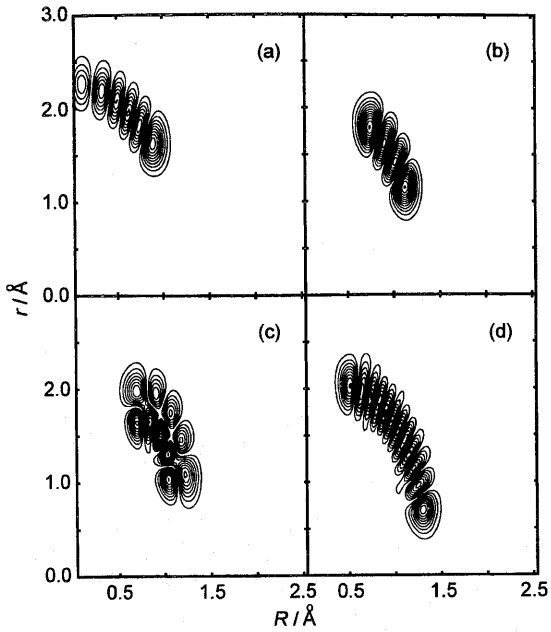

FIG. 6. Vibrational wave functions on the $R-r$ plane at $\theta=90°$ for (a) the tenth state (0,5,0) of $H_2S^+(\tilde{A})$, and (b) the sixth state (0,3,0), (c) the 23rd state (1,4,0), and (d) the 92nd state (0,11,0) of $H_2S^+(\tilde{X})$.

$$G(\nu_1,\nu_2,\nu_3)=\sum_{i=1}^{3}\omega_i^0\nu_i+\sum_{i=1}^{3}\sum_{k\geq i}^{3}x_{ik}^0\nu_i\nu_k. \quad (1)$$

In contrast, such an analysis was very unsatisfactory for the $H_2S^+(\tilde{A})$ state; the standard deviation for the lowest 55 levels was 150 cm^{-1}. We therefore introduced the third order term $y_{222}^0\nu_2^3$ in Eq. (1) since the ν_2 energies show a large anharmonicity effect. The vibrational constants obtained for a best-fitted analysis are summarized in Table V. The anharmonicity constants for $H_2S^+(\tilde{A})$ are much larger than those for $H_2S(\tilde{X})$ and $H_2S^+(\tilde{X})$, indicating that the vibrational coupling is relatively large in the $H_2S^+(\tilde{A})$ state.

The transition energy calculated for the $H_2S^+(\tilde{A}-\tilde{X})$ system is 18 600 cm^{-1}, which agrees well with the observed value of 18 520 cm^{-1} and the calculated value of 18 620 cm^{-1}.[8,26]

C. Franck–Condon factors

To evaluate the vibrational distributions of the $H_2S^+(\tilde{X}\,^2B_1,\tilde{A}\,^2A_1)$ states produced by the Penning ionization of H_2S, the FCFs were calculated for the $(\nu_1''=0,\nu_2''=0,\nu_3''=0)\rightarrow(\nu_1'\nu_2'\nu_3')$ band of the $H_2S(\tilde{X})\rightarrow H_2S^+(\tilde{X},\tilde{A})$ transition. Table VI lists the results for the $H_2S(\tilde{X})\rightarrow H_2S^+(\tilde{X})$ transition. In this transition the change in r_{SH} is only 0.02 Å, and the HSH angle does not change. Therefore, the main band is the transition to the vibrational ground state, and the FCF to the (0,0,1) state is nearly zero since its wave function has a node on the $R-r$ plane at $\theta=90°$. In contrast, the α is greatly enlarged with the $H_2S(\tilde{X})\rightarrow H_2S^+(\tilde{A})$ transition, although the r_{SH} length remains the same. Thus the bending mode (ν_2') is intensely enhanced in the ionization. Table VII summarizes the calculated results; the sum of the FCFs in the table is 0.93. The $H_2S^+(\tilde{A})$ state, which is produced directly from H_2S, may populate primarily in the $(0,\nu_2'=2-10,0)$ states according to the Franck–Condon (FC) principle. In this calculation, the population maximum is at $\nu_2'=6-7$, which is shifted higher than the peak around $\nu_2'=4-5$ observed in the photoelectron spectrum of H_2S, which is considered to be an FC type.[26,29] This discrepancy is probably caused by the dependence of the electronic transition probability on the vibrational states, which is neglected in the FCFs. Therefore, Einstein's B coefficients should be compared with the observed result. The maximum in Einstein's B coefficients, which incorporate the dependence of

TABLE III. Calculated and observed vibrational frequencies for the $H_2S(\tilde{X})$ and $H_2S^+(\tilde{X},\tilde{A})$ states and the barrier to linearity in cm^{-1} units.

State		This work[a]	Theoretical	Observed
$H_2S(\tilde{X})$	ν_1	2574	···	2614.6[c]
	ν_2	1158	···	1182.7[c]
	ν_3	2683	···	2627.5[c]
$H_2S^+(\tilde{X})$	ν_1	2503	2710[b]	2380±50,[d] 2516,[e] 2485±40[f]
	ν_2	1129	1240,[b] 1480[j]	1165,[g] ~1000[e]
	ν_3	2549	2780[b]	···
$H_2S^+(\tilde{A})$	ν_1	2463	2620[b]	2040±50[d]
	ν_2	1029	1020,[b] 1150[j]	~960,[g] 940±50,[d] 855,[e] 910±10,[f] 1088,[h] 1080[i]
	ν_3	2483	2580[b]	···
$H_2S^+(\tilde{X})$ barrier		23 100	23 470[b]	23 114[g]
$H_2S^+(\tilde{A})$ barrier		4600	4600[b]	4400[g]

[a]The difference between the first excited state and the vibrational ground state.
[b]Reference 8.
[c]Reference 26.
[d]Reference 29.
[e]Reference 30.
[f]Reference 32.
[g]Reference 28.
[h]Reference 33.
[i]Reference 34.
[j]Reference 6.

TABLE IV. Energy levels for the bending vibration of $H_2S^+(\tilde{A})$ in cm^{-1} units.

ν_2'	Calculated[a]	Observed[b]	% Difference
0	0.0	0.0	...
1	1028.5	959.35*	7.2
2	1945.5	1893.05*	2.8
3	2720.3	2790.88*	−2.5
4	3355.7	3666.23	−8.5
5	4036.6	4539.97	−11.1
6	4850.0	5445.66	−10.9
7	5756.0	6403.76	−10.1
8	6727.2	...	...
9	7745.9	...	...
10	8794.7	...	...

[a]This work.
[b]The figure with the asterisk (*) means the estimated value, Ref. 27.

the transition probability on the vibrational states for the $H_2S(\tilde{X})\rightarrow H_2S^+(\tilde{A})$ ionization, is estimated to shift to lower ν_2' than that of FCF since the transition moment is expected to be larger around the equilibrium geometry from the analogy of the $H_2S^+(\tilde{X}-\tilde{A})$ transition.

To analyze the vibrational populations of the $H_2S^+(\tilde{A}-\tilde{X})$ emission spectra resulting in the collision of He*(2 ^3S) with H_2S, the FCFs were calculated for the $(\nu_1',\nu_2',\nu_3')\rightarrow(\nu_1'',\nu_2'',\nu_3'')$ band of the $H_2S^+(\tilde{A}-\tilde{X})$ transition. The lowest 100 vibrational states of the $\tilde{A}$ state and the lowest 200 vibrational states of the $\tilde{X}$ state were included in the calculation. The $H_2S^+(\tilde{A})$ state produced from H_2S seems to be populated primarily in the $(0,\nu_2'=2-10,0)$ states, assuming an FC-type ionization. In this context, the FCFs from the $(0,\nu_2'=0-10,0)$ states are summarized in Table VIII. The $H_2S^+(\tilde{A}-\tilde{X})$ emission is expected to consist of pure bending progressions, and the contribution of the combination bands seems to be small. Although levels up to $\nu_2'=14$ were observed in the photoelectron spectrum,[32] no emissions from levels with $\nu_2'\geqslant 7$ were observed because of the predissociation of H_2S^+.[26] Table IX lists Einstein's A coefficients[25] for the vibrational bands from the $(0,\nu_2'=0-10,0)$ states. The peak in Einstein's A coefficients from each state is shifted lower than that for the corresponding FCFs because of both the dependence of the transition moment on the vibrational states and the third power of the transition energy.

TABLE V. Vibrational constants for $H_2S(\tilde{X})$ and $H_2S^+(\tilde{X},\tilde{A})$ in cm^{-1} units.

	$H_2S(\tilde{X})$	$H_2S^+(\tilde{X})$	$H_2S^+(\tilde{A})$
n[a]	56	73	55
ω_1^0	2598	2513	2583
ω_2^0	1179	1158	1102
ω_3^0	2658	2525	2533
x_{11}^0	−19	−23	−92
χ_{22}^0	−1	−1	−87
χ_{33}^0	−22	−13	−30
χ_{12}^0	5.5	−11	−38
χ_{13}^0	−114	−114	−154
χ_{23}^0	−20	−22	−44
y_{222}^0	...	...	6
σ[b]	50	44	63

[a]The number of vibrational levels included in the analysis.
[b]The standard deviation for vibrational frequencies.

TABLE VI. FCFs calculated for the $(\nu_1''=0,\nu_2''=0,\nu_3''=0)\rightarrow(\nu_1',\nu_2',\nu_3')$ band of the $H_2S(\tilde{X})\rightarrow H_2S^+(\tilde{X})$ transition.

(ν_1',ν_2',ν_3')	FCF
(0,0,0)	0.964
(0,1,0)	0.008
(1,0,0)	0.026
(0,0,1)	0.000

Although Bruna *et al.*[8] reported the FCFs for the $H_2S^+(\tilde{A}-\tilde{X})$ transition, they treated the calculation of the FCF as a one-dimensional model. Therefore, our data obtained by the three-dimensional calculation cannot be directly compared with their data; for example, the FCFs for the $(1,0,0)-(\nu_2''=0-2,0,0)$ bands are 0.0005, 0.011, and 0.0005, respectively, against 0.143, 0.959, and 0.027 in Table 6 of Ref. 8. We found that the FCFs from the (1,0,0) state of $H_2S^+(\tilde{A})$ are distributed widely among the combination states of $H_2S^+(\tilde{X})$. Thus, the one-dimensional treatment is insufficient for the vibrational states for $H_2S^+(\tilde{X},\tilde{A})$ since the vibrational coupling is relatively large. The plot of FCFs for the $\nu_2'(K'=1)-\nu_2''=0(K''=0)$ progression in Fig. 6 of Ref. 8 may be comparable to the corresponding FCFs for the $(0,\nu_2',0)-(0,0,0)$ transition in Table VIII. The data in this study have a maximum at $\nu_2'=6-7$ against a maximum at $\nu_2'=5-6$ in Ref. 8. The difference may originate in the three-dimensional treatment of FCF against the one-dimensional model of the vibrational states rather than the PES.

IV. CONCLUSION

The potential energy surfaces of $H_2S(\tilde{X})$ and $H_2S^+(\tilde{X},\tilde{A})$ were obtained from the MCSCF/MRCI method in this study. The vibrational energies were calculated for these electronic states, and the vibrational states were as-

TABLE VII. FCFs calculated for the $(0,0,0)\rightarrow(\nu_1',\nu_2',0)$ band of the $H_2S(\tilde{X})\rightarrow H_2S^+(\tilde{A})$ transition.

ν_2'	$(0,\nu_2',0)$	$(1,\nu_2',0)$	$(2,\nu_2',0)$
0	0.006	0.001	0.000
1	0.025	0.004	0.008
2	0.049	0.007	0.000
3	0.064	0.008	0.011
4	0.073	0.004	...
5	0.106	0.014	...
6	0.129	0.008	...
7	0.126	0.020	...
8	0.106	0.023	...
9	0.075	0.022	...
10	0.041	...	...

TABLE VIII. FCFs calculated for the $H_2S^+(\tilde{A}-\tilde{X})$ transitions and related vibrational energies G.

$\tilde{X}$ state	$\tilde{A}$ state (G/cm^{-1})	(0,0,0) 0	(0,1,0) 1029	(0,2,0) 1946	(0,3,0) 2720	(0,4,0) 3356	(0,5,0) 4037	(0,6,0) 4850	(0,7,0) 5756	(0,8,0) 6727	(0,9,0) 7746	(0,10,0) 8795
(0,0,0)	0	0.010	0.038	0.069	0.083	0.091	0.125	0.145	0.135	0.108	0.070	0.037
(0,1,0)	1129	0.051	0.118	0.125	0.084	0.047	0.021	0.000	0.017	0.070	0.113	0.121
(0,2,0)	2259	0.113	0.142	0.061	0.006	0.002	0.030	0.073	0.071	0.025	0.001	0.049
(0,3,0)	3421	0.162	0.081	0.000	0.024	0.051	0.063	0.025	0.001	0.049	0.078	0.029
(0,4,0)	4592	0.162	0.012	0.031	0.057	0.033	0.004	0.017	0.064	0.042	0.000	0.049
(0,5,0)	5767	0.125	0.003	0.061	0.024	0.000	0.021	0.052	0.013	0.011	0.063	0.030
(0,6,0)	6930	0.081	0.029	0.041	0.000	0.015	0.036	0.009	0.015	0.048	0.008	0.023
(0,7,0)	8073	0.049	0.050	0.012	0.010	0.025	0.012	0.005	0.038	0.006	0.019	0.038
(0,8,0)	9202	0.031	0.063	0.000	0.025	0.016	0.000	0.027	0.012	0.011	0.029	0.000
(0,9,0)	10 327	0.023	0.078	0.008	0.035	0.004	0.014	0.029	0.001	0.037	0.002	0.035
(0,10,0)	11 425	0.015	0.081	0.038	0.026	0.002	0.037	0.008	0.027	0.020	0.016	0.030
(0,11,0)	12 485	0.008	0.063	0.068	0.006	0.019	0.033	0.002	0.038	0.000	0.040	0.000
(0,12,0)	13 525	0.004	0.043	0.085	0.000	0.036	0.010	0.026	0.014	0.025	0.014	0.027
(1,0,0)	2503	0.000	0.000	0.001	0.002	0.003	0.005	0.008	0.008	0.010	0.006	0.009
(1,2,0)	4762	0.020	0.004	0.001	0.004	0.003	0.002	0.000	0.002	0.001	0.000	0.000
(1,3,0)	5940	0.032	0.000	0.012	0.008	0.001	0.002	0.009	0.010	0.000	0.004	0.000
(1,4,0)	7091	0.030	0.009	0.015	0.001	0.004	0.012	0.007	0.000	0.009	0.002	0.003
(1,5,0)	8232	0.027	0.028	0.008	0.004	0.014	0.009	0.000	0.010	0.005	0.007	0.008
(1,6,0)	9338	0.018	0.039	0.000	0.015	0.012	0.000	0.012	0.010	0.002	0.020	0.000

signed. The accuracy of the vibrational energies for $H_2S^+(\tilde{X},\tilde{A})$ is roughly estimated to be 10% up to 8000 cm^{-1}. We believe that this accuracy is adequate for calculating the FCFs for the $H_2S^+(\tilde{A}-\tilde{X})$ transition. The FCFs for the $H_2S(\tilde{X})\rightarrow H_2S^+(\tilde{A})$ ionization show that the $H_2S^+(\tilde{A})$ state primarily populates in the $(0,\nu_2'=2-10,0)$ state with a maximum around $\nu_2'=6-7$. This feature is, however, shifted higher than that of the photoelectron spectra of H_2S, which show a peak at $\nu_2'=4-5$.[26,32] For a more accurate comparison with the observed data, we need to obtain Einstein's B coefficients, which incorporate the dependence of the transition probability on the vibrational states. Even if the pure bending state of $H_2S^+(\tilde{A})$ is primarily produced, some combination states may be populated through the vibrational coupling. We found that the FCFs calculated for some combination states near the $(0,\nu_2'=2-10,0)$ states of $H_2S^+(\tilde{A})$ are dispersed among several vibrational states of $H_2S^+(\tilde{X})$. Therefore, even if any emissions from combination states do occur, they would be hidden by intense bending progressions, which is consistent with there being no emissions as-

TABLE IX. Einstein's A coefficients calculated for the $H_2S^+(\tilde{A}-\tilde{X})$ transitions.

$\tilde{X}$ state	$\tilde{A}$ state (0,0,0)	(0,1,0)	(0,2,0)	(0,3,0)	(0,4,0)	(0,5,0)	(0,6,0)	(0,7,0)	(0,8,0)	(0,9,0)	(0,10,0)
(0,0,0)	86	316	579	711	784	1083	1266	1185	946	612	296
(0,1,0)	385	899	969	655	367	166	2	138	558	884	905
(0,2,0)	770	989	428	44	17	219	542	539	196	3	313
(0,3,0)	1005	521	4	154	331	412	167	7	330	542	222
(0,4,0)	917	81	166	329	202	26	93	362	246	1	302
(0,5,0)	644	10	306	136	3	94	265	73	51	324	149
(0,6,0)	370	109	198	3	56	162	51	57	215	41	96
(0,7,0)	193	177	60	29	97	56	14	147	29	66	156
(0,8,0)	101	194	2	79	62	0	87	50	31	105	0
(0,9,0)	56	193	16	95	14	34	92	1	112	11	100
(0,10,0)	27	154	71	60	2	83	24	61	59	37	88
(0,11,0)	10	89	100	13	29	62	3	77	0	86	0
(0,12,0)	3	44	93	0	45	17	34	26	35	27	43
(1,0,0)	0	0	1	4	8	12	19	24	3	13	32
(1,2,0)	74	8	11	28	14	4	5	33	13	0	11
(1,3,0)	113	3	60	30	0	18	60	50	4	44	4
(1,4,0)	96	40	59	1	21	57	27	0	56	8	26
(1,5,0)	73	93	23	17	55	32	3	45	20	39	47
(1,6,0)	39	105	0	48	36	0	46	33	11	79	0

signed from combination state.[28] These findings indicate that the vibrational distribution of $H_2S^+(\tilde{A})$ obtained from the analysis of emission spectra is not deviated by combination bands.

ACKNOWLEDGMENTS

This work was supported by a Grant-in-Aid from the Ministry of Education, Science, and Culture (Grant Nos. 11640499 and 13740336) and by the Joint Research Program of IMS.

[1] V. Čermák and A. J. Yencha, J. Electron Spectrosc. Relat. Phenom. **11**, 67 (1977).
[2] C. E. Brion and D. S. C. Lee, J. Electron Spectrosc. Relat. Phenom. **12**, 77 (1977).
[3] K. Mitsuke, T. Takami, and K. Ohno, J. Chem. Phys. **91**, 1618 (1989).
[4] M. Tsuji, K. Tsuji, H. Fukutome, and Y. Nishimura, Chem. Lett. **1977**, 673.
[5] A. J. Yencha and K. T. Wu, Chem. Phys. **32**, 247 (1978).
[6] H. Sakai, S. Yamabe, T. Yamabe, and K. Fukui, Chem. Phys. Lett. **25**, 541 (1974).
[7] G. Hirsch and P. J. Bruna, Int. J. Mass Spectrom. Ion Phys. **36**, 37 (1980).
[8] P. J. Bruna, G. Hirsch, M. Perić, S. D. Peyerimhoff, and R. J. Beunker, Mol. Phys. **40**, 521 (1980).
[9] D. E. Woon and T. H. Dunning, Jr., J. Chem. Phys. **98**, 1358 (1993), and references therein.
[10] M. R. A. Blomberg and P. E. M. Siegbahn, J. Chem. Phys. **78**, 5682 (1988).
[11] J. Simons, J. Phys. Chem. **93**, 626 (1989).
[12] S. R. Langhoff and D. E. Davidson, Int. J. Quantum Chem. **8**, 61 (1974).
[13] H.-J. Werner and P. J. Knowles, J. Chem. Phys. **89**, 5803 (1988).
[14] P. J. Knowles and H.-J. Werner, Chem. Phys. Lett. **145**, 514 (1988).
[15] MOLPRO is a package of *ab initio* programs written by H.-J. Werner and P. J. Knowles with contributions from R. D. Amos *et al.*
[16] D. Shepard, Proceedings ACM National Conference 1968, p. 517; P. Lancaster and K. Salkauskas, *Curve and Surface Fitting, An Introduction* (Academic, London, 1986), Chap. 10.
[17] K. C. Thompson, M. J. T. Jordan, and M. A. Collions, J. Chem. Phys. **108**, 8302 (1998) and references therein.
[18] T. Ishida and G. C. Schatz, Chem. Phys. Lett. **314**, 369 (1999).
[19] J. V. Lill, G. A. Parker, and J. C. Light, Chem. Phys. Lett. **89**, 483 (1982).
[20] D. T. Colbert and W. H. Miller, J. Chem. Phys. **96**, 1982 (1992).
[21] E. M. Goldfield and S. K. Gray, Comput. Phys. Commun. **98**, 1 (1998).
[22] C.-Y. Yang and S. K. Gray, J. Chem. Phys. **107**, 7773 (1997).
[23] J. Tennyson and B. T. Sutcliffe, J. Chem. Phys. **77**, 4061 (1982).
[24] R. B. Lehoucq, K. Maschhoff, D. C. Sorensen, and C. Yang, ARPACK (Rice University, Houston, 1997); see the ARPACK homepage, http://www.caam.rice.edu/software/ARPACK/
[25] H. Eyring, J. Walter, and G. E. Kimball, *Quantum Chemistry* (Wiley, New York, 1944), p. 115.
[26] R. N. Dixon, G. Duxbury, M. Horani, and J. Rostas, Mol. Phys. **22**, 977 (1971).
[27] G. Herzberg, *Molecular Spectra and Molecular Structure*, Electronic Spectra and Electronic Structure of Polyatomic Molecules, Vol. 3 (Van Nostrand, Princeton, 1966).
[28] G. Duxbury, M. Horani, and J. Rostas, Proc. R. Soc. London, Ser. A **331**, 109 (1972).
[29] D. W. Turner, C. Baker, A. D. Baker, and C. R. Brundle, *Molecular Photoelectron Spectroscopy* (Wiley-Interscience, New York, 1970).
[30] J. Delwiche, P. Natalis, and J. E. Collins, Int. J. Mass Spectrom. Ion Phys. **5**, 443 (1970); J. Delwiche and P. Natalis, Chem. Phys. Lett. **5**, 564 (1970).
[31] A. W. Potts and W. C. Price, Proc. R. Soc. London, Ser. A **326**, 181 (1972).
[32] L. Karlsson, L. Mattsson, R. Jardny, T. Bergmark, and K. Siegbahn, Phys. Scr. **12**, 229 (1976).
[33] D. C. Frost, A. Katrib, C. A. McDowell, and R. A. N. McLean, Int. J. Mass Spectrom. Ion Phys. **7**, 485 (1971).
[34] S. Durmaz, G. H. King, and R. J. Suffolk, Chem. Phys. Lett. **13**, 304 (1972).